DOI:
10.2967/jnumed.115.164384

Document Version
Peer reviewed version

c-Met PET Imaging Detects Early Stage Loco-Regional Recurrence of Basal-Like Breast Cancer

Appitha Arulappu[1*], Mark Battle[2*], Michel Eisenblaetter[1,3,4*], Graeme McRobbie[2], Imtiaz Khan[2], James Monypenny[1], Gregory Weitsman[1], Myria Galazi[1], Susan Hoppmann[2], Patrycja Gazinska[5], Wulan Wulaningsih[1], Grethe Tang Dalsgaard[2], Sven Macholl [2, 6**], Tony Ng[1,5,7**]

1. Richard Dimbleby Department of Cancer Research, Kings College London, London, UK

2. GE Healthcare, Life Sciences, Amersham, UK

3. Division of Imaging Sciences & Biomedical Engineering, King's College London, London, UK

4. Department of Clinical Radiology, University Hospital Münster, Münster, Germany

5. Breast Cancer NOW Unit, King's College London School of Medicine, London, UK

6. Barts Cancer Institute, Queen Mary University of London, London, UK

7. UCL Cancer Institute, University College London, London, UK

* Contributed equally to this work

** Co-senior authors

Corresponding author:

Professor Tony Ng

The Richard Dimbleby Department of Cancer Research

New Hunt's House

Guy's Hospital Campus

London SE1 1UL, UK

E-mail: tony.ng@kcl.ac.uk

Telephone: +44 (0)207 848 8056 Fax: +44 (0)20 7848 6220

Short running title:

cMet imaging of loco-regional recurrence

ABSTRACT

Loco-regional recurrence of breast cancer poses significant clinical problems due to frequent inoperability once the chest wall is involved. Early detection of recurrence by molecular imaging agents against therapeutically targetable receptors, such as c-Met, would be of potential benefit. The aim of this study was to assess [^{18}F]AH113804,a peptide-based molecular imaging agent with high affinity for human c-Met, for the detection of early-stage loco-regional recurrence in a human basal-like breast cancer model, HCC1954. **Methods:** HCC1954 tumor-bearing xenograft models were established, and [^{18}F]AH113804 was administered. Distribution of radioactivity was determined via positron emission tomography (PET) at 60 min post radiotracer injection. PET and CT (computerized tomography) images were acquired 10 days after tumor inoculation, to establish baseline distribution and uptake, and then on selected days after surgical tumor resection. CT images and caliper were used to determine the tumor volume. Radiotracer uptake was assessed by [^{18}F]AH113804 PET imaging. c-Met expression was assessed by immunofluorescence imaging of tumor samples and correlated with [^{18}F]AH113804 PET imaging results. **Results:** Baseline uptake of [^{18}F]AH113804, determined in tumor-bearing animals after 10 days, was approximately 2-fold higher in the tumor as compared to muscle tissue or the contralateral mammary fat pad. The tumor growth rate, determined from CT images, was comparable between the animals with recurrent tumors, with detection of tumors of low volume (<10 mm^3) only possible by Day 20 post tumor resection. [^{18}F]AH113804 PET detected local tumor recurrence as early as six days after surgery in the recurrent tumor-bearing animals, and exhibited significantly higher [^{18}F]AH113804 uptake (in comparison to mammary fatty tissue) with a target to background (muscle) ratio of approximately 3:1 (p<0.01). The c-Met expression of individual resected tumor samples, determined by immunofluorescence, correlated with the respective [^{18}F]AH113804 imaging signals (r=0.82; p<0.05). **Conclusion:** [^{18}F]AH113804 PET provides a new diagnostic tool for the detection of c-Met-expressing primary tumor and has potential utility for the detection of loco-regional recurrence from an early stage.

Keywords

PET/CT imaging, basal-like breast cancer, HCC1954, c-Met, AH113804, cancer, loco-regional recurrence

INTRODUCTION

The proto-oncogene c-Met is a receptor tyrosine kinase activated by the ligand hepatocyte growth factor (HGF). The HGF/c-Met signaling axis has been described as a promoter of cancer cell growth, angiogenesis, invasion and metastasis (*1*). Overexpression of c-Met is associated with poor prognosis and a more malignant tumor phenotype (*2,3*). Several c-Met inhibitors are currently under evaluation in clinical trials, either as stand-alone therapies or in concomitant treatment (*4*). c-Met is overexpressed in various solid tumors (*5*), including breast cancer (BC), with higher expression in Basal-like Breast Cancer (BLBC) than in other intrinsic cancer subtypes (*6*) . BLBC, which accounts for up to 15% of all BCs, exhibits a high rate of loco-regional recurrence after initial therapy (*7-10*).

Although treatment of localized disease has improved over the past decades, up to 45% of BC patients suffer a local, regional or systemic relapse within 8 years after initial therapy (*8*). While systemic relapse in the form of distant metastasis is still regarded as incurable according to current treatment guidelines, loco-regional recurrence of BC should be treated with curative intention (*11*). Treatment success crucially depends on the earliest possible diagnosis, before chest wall involvement or further organ invasion prevents any form of aggressive treatment (*12*). Established guidelines for post-therapy monitoring in BLBC feature mammography and clinical examination which frequently fail to identify local tumor relapse at a sufficiently early stage (*13*).

Magnetic resonance imaging (MRI) and FDG-PET/CT offer a comparably higher sensitivity and specificity for detection and characterization of BC relapse (*14*). However, differentiation of recurrent BC from inflammatory or infectious processes, and the identification of small lesions (tumor size <20 mm) still impose challenges for FDG-PET (*15,16*). c-Met targeted imaging could provide such a tool to further improve the performance of post-treatment surveillance, and could aid patient stratification for targeted therapy.

For this study we chose the novel, peptide-based molecular imaging agent [^{18}F]AH113804 (Fig 1A) which binds to human c-Met with high affinity (*K*d≈2 nM), has a favorable kinetic profile, exhibits specific uptake in c-Met positive tumor tissue and rapid systemic clearance (*17*). This enables for diagnostic PET imaging as early as one hour after administration (*17*). The safety, pharmacokinetics and imaging characteristics have all been assessed using GE-137, the fluorescent-labelled analogue of AH113804, in healthy volunteers and in patients at high risk of colorectal

neoplasia (*17*).These initial studies in humans suggested that GE-137 was safe, and that it may improve visualization of colonic polyps, which display a high level for c-Met (*17*).

In this study, we assessed [^{18}F]AH113804-driven PET for the early detection of loco-regional tumor recurrence in a preclinical model of BLBC.

MATERIALS AND METHODS

Cell culture

Human basal-like subtype breast cancer cells HCC1954 (CRL-2338) were obtained from the American Type Culture Collection and cultured in RPMI 1640 (Invitrogen) with 10% fetal calf serum (Bodinco BV) and 2 mM L-glutamine (Invitrogen) at 37 °C in a fully humidified atmosphere containing 5% CO_2.

Western blotting

Immunoblotting was performed as described in ref (*18*). Detection of bound antibody was with horseradish peroxidase-conjugated secondary antibodies and enhanced chemiluminescence (ThermoScientifc Fisher) with G-Box, Syngene.

Tumor xenograft model

All animal studies were performed in compliance with the UK Home Office Animals (Scientific Procedures) Act 1986. Female SCID (Severely Immunodeficient) mice (17 to 19 g at time of first procedure, Charles River UK) were subcutaneously injected with 4×10^6 cells in 0.1 mL of a 1:1 mixture of medium and Matrigel (BD Biosciences) in the second right mammary fat pad. Tumor size was measured twice per week by caliper. The volume for the tumor was estimated as length*width^2/2. Further details on the tumor xenograft model are given in the Supplementary Methods.

Radiosynthesis of [^{18}F]AH113804

Synthesis of the peptide is described in the supplementary section of ref (*17*). Details of the radiosynthesis of [^{18}F]AH113804 are given in the Supplementary Methods.

CT and PET imaging

Small-animal PET/CT imaging was performed using microPET P4 (Concorde) and microCAT II (ImTek Inc.) systems as described earlier (*19*). Each animal was injected intravenously (iv) with approximately 7 MBq (0.1 mL) [^{18}F]AH113804. Further details of the imaging procedure are given in the Supplementary Methods.

Tumor and contralateral mammary fat pad uptake are presented as target-to-muscle retention ratio (TMRR). Further details are given in the Supplementary Methods.

Ex vivo tissue analyses

Details of all ex vivo tissue analyses are given in the Supplementary Methods. These include histology of formalin-fixed, paraffin-embedded tumor and quadriceps muscle, and [^{18}F]AH113804 autoradiography and immunofluorescence staining of snap-frozen tumor tissue.

Statistical analysis

Unless otherwise stated, group averaged data are presented as mean ± standard error of the mean (SEM). The observed skewed distribution of TMRR measures was lessened by logarithmic transformation, see Supplementary Methods. All statistical analyses were performed in R version 3.1.2 (R Project for Statistical Computing, Vienna, Austria).

RESULTS

Synthesis of [^{18}F]AH113804

Total synthesis time on the automated platform was 49 min. For all synthesis runs, the decay corrected end-of-synthesis yield was between 38 and 41%, with a radioactive concentration (RAC) between 600 and 800 MBq/mL. The radiochemical purity was always >90%, the chemical content between 15 and 20 µg/mL, and specific activity approximately 100 GBq/µmol for each test item.

c-Met expression level in HCC1954

Human c-Met protein expression level was assessed in HCC1954, compared to HT-29 (high c-Met expressing) and U87 (moderate c-Met expressing) cell line lysates. The data shows upregulation of c-Met in the HCC1954 cell line (Suppl Fig 1). Burggraff *et al*. assessed the specificity

of GE-137, performing a competition study in HT-29 tumor bearing mice which showed a reduction in tumor uptake of GE-137 when co-administrated with an excess of unlabeled peptide (*17*).

Tumor targeting of [^{18}F]AH113804

Baseline uptake of [^{18}F]AH113804 (Fig 1A) was assessed in 8 tumor-bearing animals using PET imaging at 10 days post tumor inoculation (Fig. 1B). Levels of radioactivity at 60 minutes pi were 4.9±0.6% ID/mL in kidney, 2.9±0.3% ID/mL in liver, and 2.0±0.2% ID/mL in blood. PET imaging (Fig 1C) revealed a significant difference between the uptake of [^{18}F]AH113804 at the tumor site (1.5±0.2% ID/mL, white arrowhead) compared to both contralateral mammary fat pad (0.8±0.1% ID/mL, blue arrowhead) and muscle (0.8±0.1% ID/mL) at 60 minutes p.i. *Ex vivo* biodistribution studies, following PET imaging on Day 50 post tumor resection, confirmed [^{18}F]AH113804 accumulation in tumor was significantly higher compared to muscle (2.5±0.6% ID/g *vs*. 0.9±0.2%ID/g at 70 min pi, n=3. p<0.05. Suppl Fig 2).

Early-stage recurrent tumor growth is first detected with [^{18}F]AH113804, later by CT, and last by palpation

Following tumor resection 14 to 16 days after inoculation, 5 animals were found to exhibit recurrent tumor growth, confirmed by necropsy after final imaging. The remaining 3 animals did not exhibit any tumor re-growth (by caliper measurements). However, there was lack of correlation between tumor size by caliper and uptake of the tracer at the tumor site (Suppl Fig. 3). Tissue from the site of injection for one of the non-recurrent mice was stained. Negativity for tumor cells and human c-Met expression by IHC was confirmed (Suppl Fig. 4). In this case, the %ID/g in the ROI was 0.6 (c.f. the %ID/g at the contralateral site was 0.5).

Analysis of [^{18}F]AH113804 PET images provided evidence for the presence of loco-regional recurrence from Day 6 post-resection in these 5 animals (Figure 2A). There was some degree of variation in the uptake of radioactivity at the tumor site in individual animals on each study day (Suppl Table 1). However, overall uptake on each day was comparable to that observed in the tumors pre-resection. The TMRR was significantly higher at the tumor resection site in comparison to the contralateral mammary fat pad on Day 6 (2.7±0.3 *vs*. 1.0±0.3, p<0.001; n=5; Fig 2B). Uptake of [^{18}F]AH113804 at the site of resection remained clearly visible in the PET images on subsequent

days, with the TMRR significantly smaller in the contralateral mammary fat pad on Day 13 (1.6±0.2 vs 0.9±0.2, p<0.01), Day 20 (1.6±0.1 vs 0.9±0.2, p<0.001) and Day 36 (1.5±0.8 vs 0.9±0.2, p<0.01). At Day 50 post tumor resection, the TMRR was also higher for the tumor site (1.7±0.7) than for the contralateral mammary fat pad (1.0±0.0), although this difference was not statistically significant. No specific [^{18}F]AH113804 retention was detected in the contralateral mammary fat pad with levels of radioactivity in this region comparable to muscle tissue for all time points (Suppl Fig 5).

By Day 20 post tumor resection, the mean tumor volume determined by CT measurement was approximately 7.0±12.5 mm^3 (Fig 3A&B). Palpable tumor recurrence was detected from Day 29 post tumor resection (Fig 3A).

[^{18}F]AH113804 retention in tumor tissue versus systemic clearance

Systemic clearance of [^{18}F]AH113804 was studied in selected tumor-bearing mice over the first 60 min pi by dynamic PET imaging. Figure 4A shows the distribution of [^{18}F]AH113804 at 15 min (13-18 min) and 60 min (55-65 min) p.i. A decrease in [^{18}F]AH113804 signal is observed in the major perfused organs, and retention of [^{18}F]AH113804 at the tumor site (Fig 4B).

Figure 4C displays the change in TMRR from 5 min to 60 min pi in relation to TMRR at 5 min p.i. While the tumor TMRR continuously increased, TMRRs for lungs, liver, heart and others decreased.

Autoradiography and immunohistochemical analysis confirm [^{18}F]AH113804 accumulation in c-Met positive tumor tissues

A heterogeneous pattern of [^{18}F]AH113804 distribution was observed within the tumor, with viable tissue in the tumor periphery exhibiting a positive signal while the central tumor regions exhibited only low activity (Figure 5A). H&E staining and immunohistochemistry of consecutive tumor slides revealed a large number of c-Met positive tumor cells (Figure 5B, left and right panels respectively). Both recurrent and primary tumors showed necrotic areas in H&E devoid also of c-Met (IHC) and displaying low [^{18}F]AH113804 uptake (Suppl. Fig 6&7).

***Ex vivo* histology correlates with the PET images**

Following immunofluorescent staining (Figure 6A), c-Met expression levels were quantified across whole tumor slides (Figure 6B).A significant correlation was found between c-Met expression

and *in vivo* PET (r =0.82, p=0.023. n=7), suggesting [^{18}F]AH113804 signal in tumor at 60 min pi to be representative of c-Met expression. A similar correlation was observed between c-Met expression determined by IHC and [^{18}F]AH113804 signal *in vivo* (r=0.83, p=0.0015) (Suppl Fig 8).

In addition, it was found that the variation in the c-Met expression levels observed across the tumor samples (displayed in Fig 6B) was due to the tumor size. Indeed, a correlation (r = 0.83; p = 0.0005) was identified between the total c-Met intensity level and the surface area of the tumor sample (Suppl. Fig 9).

DISCUSSION

Early detection and identification of tumor relapse enables improved loco-regional recurrence control resulting in an increased quality of life and better overall survival for BC patients (*20*). Current surveillance guidelines have been shown to be less effective in the detection of loco-regional recurrence than the more expensive, yet more sensitive, approaches such as MRI or radionuclide imaging (Single-photon emission computed tomography, PET) (*13,14*). It is believed that either individually, or as a companion test for established diagnostic approaches, targeted molecular imaging of specific tumor markers bears the potential to positively change BC follow-up; especially in patients presenting with a high risk of relapse such as BLBC patients (*20,21*).

[^{18}F]AH113804 is known to have a high affinity for human c-Met, as demonstrated in studies by Evans *et al*., where the *in vivo* affinity of [^{18}F]AH113804 was determined via receptor blocking in HT-29 xenograft tumour mouse models (*22*) . [^{18}F]AH113804 clears fast from plasma and non-target tissues (such as liver, lungs and heart), allowing for high contrast imaging after injection, and improving the sensitivity for tumor detection, as confirmed by PET imaging in this study.

Our study shows that [^{18}F]AH113804-driven PET imaging allowed for early detection of loco-regional tumor recurrence in HCC1954 tumor-bearing mice after surgery. [^{18}F]AH113804 uptake and retention in the lungs and heart, reflecting the non-specific blood pool distribution of [^{18}F]AH113804 decreased constantly over the observation period. In contrast, a constant signal was observed within the region of tumor regrowth, indicative of specific accumulation of [^{18}F]AH113804 due to target

binding. [^{18}F]AH113804 allows for excellent tissue penetration, and the *in vivo* PET imaging revealed satisfactory tumor to non-target (muscle) tissue ratio from one hour p.i.

We were able to detect statistically significant differences in tumor uptake compared to contralateral mammary fat pad at Days 6, 13, 20 and 36 after tumor resection. The lack of statistical significance at the latter timepoints is most likely due to the lower, inhomogenous distribution of radioactivity in the tumors. PET images from some of those recurrent tumor bearing animals (images not shown) showed evidence of peripheral uptake only, indicative of necrosis in the tumor core.

Currently [^{18}F]FDG is used in PET diagnostics for detection and staging in cancer. Numerous studies have revealed that other, more target-specific tracers would be beneficial for the detection of loco-regional recurrence (*23*). In a study of patients with breast cancer, it was shown that tumour size was an important factor when correctly diagnosing patients (*24*). A review of 111 patients showed that a tumor size of less than 10 mm was a significant predictor of a false negative [^{18}F]FDG PET result (*16*). In our study, a specific signal from [^{18}F]AH113804 could be detected, even when the recurrent tumor was not yet observable via CT. A previous study by Cullinane *et al.* found [^{18}F]FLT to be superior over [^{18}F]FDG in assessing the effect of the c-Met inhibitor crizotinib in human glioblastoma and human gastric cancer pre-clinical models (*25*). When tumor size decreased within 1 week of treatment, [^{18}F]FDG uptake remained unchanged while [^{18}F]FLT PET showed a marked decrease in uptake. [^{18}F]FLT is reflective of cell proliferation, and as such was indicative of tumor therapy response. Still the use of [^{18}F]FLT as a marker for proliferation has been heavily debated, with reports suggesting that results should be viewed with caution (*26*). Such studies denote the importance of targeting radiotracers such as [^{18}F]AH113804 for accurate tumor detection and patient monitoring.

Our study demonstrates correlation between c-Met from the tumor samples and the maximum uptake (% ID/mL) from [^{18}F]AH113804 at those sites in the corresponding PET images. A recent study using an optical analogue of AH113804 (GE-137) also showed a good concordance between the expression of c-Met and the optical signal detected (*17,27*).

Other groups have investigated the use of both monoclonal antibodies and anticalins as probes for c-Met imaging. ^{89}Zr-db-/^{76}Br-ornartuzumab and ^{89}Zr-PRS-110 were developed and assessed for visualization of c-Met positive tumors in preclinical models (*28,29*). Optimal imaging time points were identified to be between 2 and 5 days after tracer administration, thus hampering potential routine clinical use as diagnostic agents. In contrast, the biodistribution of [^{18}F]AH113804 permitted early imaging after tracer administration. Similarly, Li *et al*. explored the use of c-Met targeting scFv-cys dimers in Non-Small Cell Lung Cancer xenografts. Despite showing very high affinity for c-Met, good contrast immunoPET imaging was achieved only at 20 hours after injection (*30*).

The ubiquity of c-Met dysregulation in malignant disease and its known influence on tumor progression make c-Met an attractive target for diagnostic targeting and therapeutic intervention in multiple cancer types. Phase II and III clinical studies, evaluating c-Met inhibition in gastroesophageal cancer, lung cancer and hepatocellular carcinoma have shown encouraging results with clear benefit for the individual patient (*4,31,32*).

It is hypothesized for BC, as well as for those cancer types that react more favourably to c-Met inhibition, that stratification of patients according to aberration in the c-Met axis resulting in target overexpression would strongly increase the efficiency of targeted treatment.
[^{18}F]AH113804 mediated PET signals proved to reflect the c-Met expression in individual tumors in our BC model, suggesting that this tracer could also serve as such a companion diagnostic for patient selection and for therapeutic purposes. Future studies to evaluate this utility are required.

CONCLUSION

This study demonstrates that [^{18}F]AH113804 PET provides a new diagnostic tool for the detection of c-Met-expressing primary tumor and has potential utility for the detection of loco-regional recurrence from an early stage. Further preclinical work is warranted to determine whether [^{18}F]AH113804 uptake in the regrowth provides a useful predictive tool for anti-c-Met therapeutic intervention.

ACKNOWLEDGMENTS

We thank GE Healthcare for the provision of [^{18}F]AH113804, and for providing access to their laboratory facilities and staff. In particular, we thank Joanne Nesbitt, Rochelle Lear, David Gendle and Chris Beazley (all GE Healthcare at the time of study) for excellent technical support. We also like to thank Sven Macholl and Mark Battle (both GE at the time of study) for both excellent technical and intellectual support. We thank Anthony Cheung and Fabian Flores-Borja (both KCL) for preparatory experiments.

This work was supported by a MRC UK/GE Healthcare CASE studentship to Appitha Arulappu, MR/L001640/1 to Michael Eisenblaetter, FP7-HEALTH-2010 grant 'Imagint' (number 259881) to Gregory Weitsman, CR-UK/EPSRC funding for the KCL-UCL CCIC (C1519/A10331, C1519/A16463; Myria Galazi, Michael Eisenblaetter), an endowment fund from Dimbleby Cancer Care to KCL (Tony Ng, James Monypenny), and a Breakthrough Breast Cancer fund to Patrycja Gazinska.

REFERENCES

1. Birchmeier C, Birchmeier W, Gherardi E, et al. Met, metastasis, motility and more. *Nat Rev Mol Cell Biol.* 2003;4:915-925.

2. Bean J, Brennan C, Shih JY, et al. Met amplification occurs with or without T790M mutations in EGFR mutant lung tumors with acquired resistance to gefitinib or erlotinib. *Proc Natl Acad Sci U S A.* 2007;104:20932-20937.

3. Rong S, Segal S, Anver M, et al. Invasiveness and metastasis of NIH 3T3 cells induced by Met-hepatocyte growth factor/scatter factor autocrine stimulation. *Proc Natl Acad Sci U S A.* 1994;91:4731-4735.

4. https://clinicaltrials.gov/ct2/show/NCT01186991. Study evaluating the safety and efficacy of onartuzumab (Metmab) and/or bevacizumab in combination with paclitaxel in patients with metastatic, triple negative breast cancer. Aug 2010.

5. Bandla S, Pennathur A, Luketich JD, et al. Comparative genomics of esophageal adenocarcinoma and squamous cell carcinoma. *Ann Thorac Surg.* 2012;93:1101-1106.

6. Gastaldi S, Comoglio PM, Trusolino L. The Met oncogene and basal-like breast cancer: another culprit to watch out for? *Breast Cancer Res.* 2010;12:208-217.

7. Dent R, Trudeau M, Pritchard KI, et al. Triple-negative breast cancer: clinical features and patterns of recurrence. *Clin Cancer Res.* 2007;13:4429-4434.

8. Lowery AJ, Kell MR, Glynn RW, et al. Locoregional recurrence after breast cancer surgery: a systematic review by receptor phenotype. *Breast Cancer Res Treat.* 2012;133:831-841.

9. Pogoda K, Niwinska A, Murawska M, et al. Analysis of pattern, time and risk factors influencing recurrence in triple-negative breast cancer patients. *Med Oncol.* 2013;30:388-395.

10. Eiermann W, Vallis KA. Locoregional treatments for triple-negative breast cancer. *Ann Oncol.* 2012;23:(Suppl 6):vi30-34.

11. Wapnir IL, Anderson SJ, Mamounas EP, et al. Prognosis after ipsilateral breast tumor recurrence and locoregional recurrences in five national surgical adjuvant breast and bowel project node-positive adjuvant breast cancer trials. *J Clin Oncol.* 2006;24:2028-2037.

12. Voogd AC, van Oost FJ, Rutgers EJ, et al. Long-term prognosis of patients with local recurrence after conservative surgery and radiotherapy for early breast cancer. *Eur J Cancer.* 2005;41:2637-2644.

13. Montgomery DA, Krupa K, Cooke TG. Alternative methods of follow up in breast cancer: a systematic review of the literature. *Br J Cancer.* 2007;96:1625-1632.

14. Schneble EJ, Graham LJ, Shupe MP, et al. Current approaches and challenges in early detection of breast cancer recurrence. *J Cancer.* 2014;5:281-290.

15. Schneble EJ, Graham LJ, Shupe MP, et al. Future directions for the early detection of recurrent breast cancer. *J Cancer.* 2014;5:291-300.

16. Kumar R, Chauhan A, Zhuang H, et al. Clinicopathologic factors associated with false negative FDG-PET in primary breast cancer. *Breast Cancer Res Treat.* 2006;98:267-274.

17. Burggraaf J, Kamerling IM, Gordon PB, et al. Detection of colorectal polyps in humans using an intravenously administered fluorescent peptide targeted against c-Met. *Nat Med.* 2015;21:955-61.

18. Ng T, Shima D, Squire A, et al. PKCalpha regulates beta1 integrin-dependent cell motility through association and control of integrin traffic. *EMBO J.* 1999;18:3909-3923.

19. Battle MR, Goggi JL, Allen L, et al. Monitoring tumor response to antiangiogenic sunitinib therapy with 18F-fluciclatide, an 18F-labeled alphaVbeta3-integrin and alphaV beta5-integrin imaging agent. *J Nucl Med.* 2011;52:424-430.

20. Meyers MO, Klauber-Demore N, Ollila DW, et al. Impact of breast cancer molecular subtypes on locoregional recurrence in patients treated with neoadjuvant chemotherapy for locally advanced breast cancer. *Ann Surg Oncol.* 2011;18:2851-2857.

21. Sohn YJ, Jang JS, Choi SR, et al. Early detection of recurrence after endoscopic treatment for early gastric cancer. *Scand J Gastroenterol.* 2009;44:1109-1114.

22. Evans P BM, Getvoldsen G, McRobbie G, et al. Nonclinical tumor efficacy studies of [18F]AH113804, a novel PET imaging agent with high affinity for the human c-Met receptor [Abstract]. . *Proceedings of the AACR 103rd Annual Meeting 2012 31 Mar – 4 Apr 2012, Chicago, IL.* 2012.

23. Gaeta CM, Vercher-Conejero JL, Sher AC, et al. Recurrent and metastatic breast cancer PET, PET/CT, PET/MRI: FDG and new biomarkers. *Q J Nucl Med Mol Imaging.* 2013;57:352-366.

24. Vallabhajosula S. (18)F-labeled positron emission tomographic radiopharmaceuticals in oncology: an overview of radiochemistry and mechanisms of tumor localization. *Semin Nucl Med.* 2007;37:400-419.

25. Cullinane C, Dorow DS, Jackson S, et al. Differential (18)F-FDG and 3'-deoxy-3'-(18)F-fluorothymidine PET responses to pharmacologic inhibition of the c-Met receptor in preclinical tumor models. *J Nucl Med.* 2011;52:1261-1267.

26. McKinley ET, Ayers GD, Smith RA, et al. Limits of [18F]-FLT PET as a biomarker of proliferation in oncology. *PLoS One.* 2013;8:e58938.

27. Liu S, Zheng Y, Volpi D, et al. Toward operative in vivo fluorescence imaging of the c-Met proto-oncogene for personalization of therapy in ovarian cancer. *Cancer.* 2015;121:202-213.

28. Jagoda EM, Lang L, Bhadrasetty V, et al. Immuno-PET of the hepatocyte growth factor receptor Met using the 1-armed antibody onartuzumab. *J Nucl Med.* 2012;53:1592-1600.

29. Terwisscha van Scheltinga AG, Lub-de Hooge MN, Hinner MJ, et al. In vivo visualization of MET tumor expression and anticalin biodistribution with the MET-specific anticalin 89Zr-PRS-110 PET tracer. *J Nucl Med.* 2014;55:665-671.

30. Li K, Tavare R, Zettlitz KA, et al. Anti-MET immunoPET for non-small cell lung cancer using novel fully human antibody fragments. *Mol Cancer Ther.* 2014;13:2607-2617.

31. https://clinicaltrials.gov/ct2/show/NCT01147484. A Study of Foretinib in Patients With Recurrent/Metastatic Breast Cancer (IND197). May 2010.

32. https://clinicaltrials.gov/show/NCT01738438. Cabozantinib for Metastatic Triple Negative BrCa. Institute D-FC. Nov 2012.

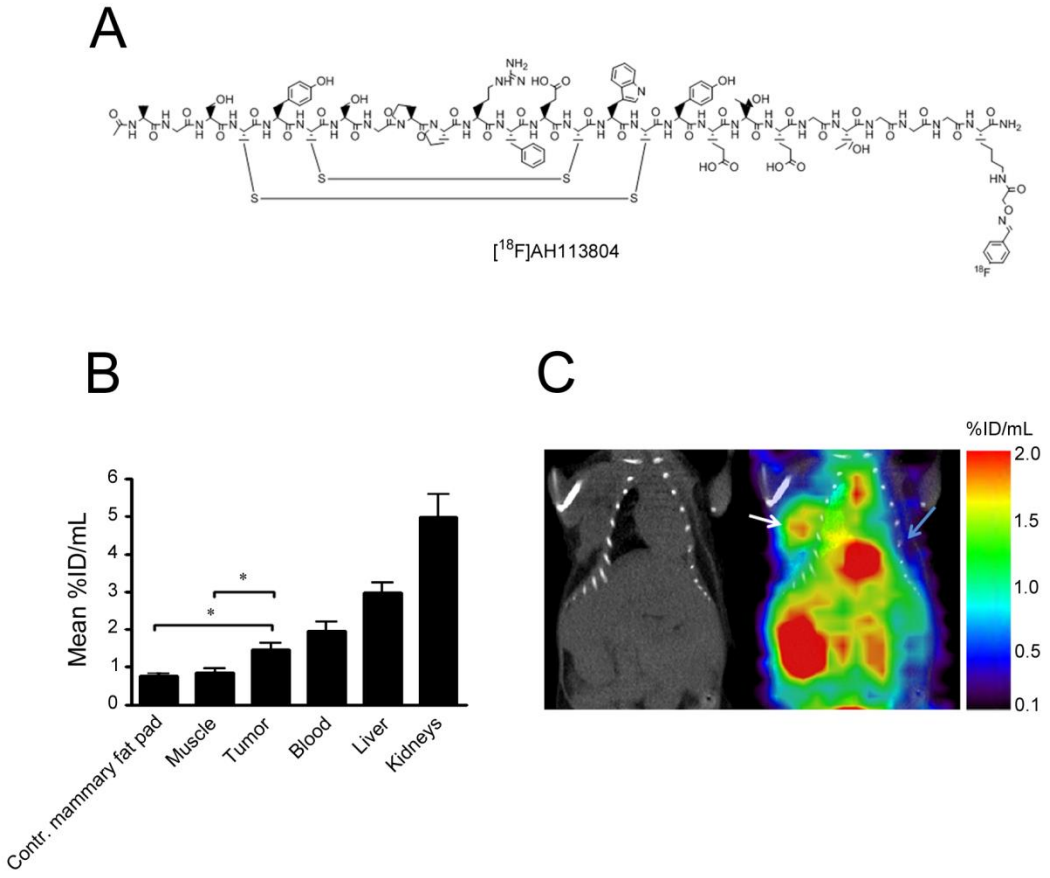

Figure 1. Biodistribution of [^{18}F]AH113804 and HCC1954 tumor. (A) Molecular structure of [^{18}F]AH113804. **(B)** Distribution of [^{18}F]AH113804 in selected organs and tissues in HCC1954 tumor xenografts 10 days p.i. Statistically significant differences were observed in the uptake of [^{18}F]AH113804 in tumor versus muscle and contralateral side (Students *t*-test, mean±SEM, n=8, *: $p<0.05$). **(C)** CT and PET/CT images of a representative tumor-bearing mouse 10 days p.i. demonstrates [^{18}F]AH113804 signal at the tumor site (white arrow), but not at the contralateral site (blue arrow).

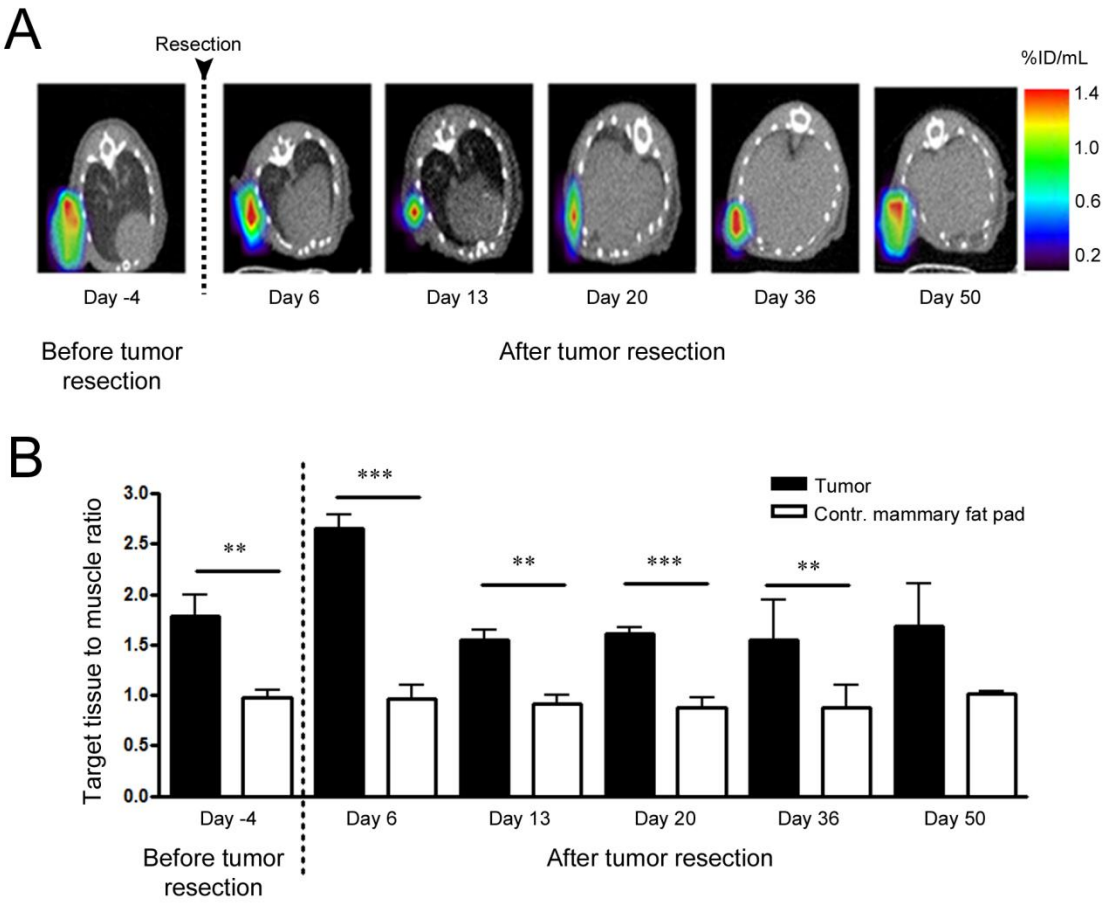

Figure 2. Early detection of tumor regrowth using [^{18}F]AH113804 for PET imaging. (A) PET/CT images of a transverse section of a representative tumor-bearing mouse, 4 days before tumor resection and at selected days after resection, show [^{18}F]AH113804 signal at the tumor site at 60 min p.i. For clarity, the PET signal only in the ROI is shown. **(B)** Target-to- muscle ratio in the tumor and contralateral sites. Statistically significant differences between both sites observed at Days 6, 13, 20 and 36 (Students *t*-test, mean±SEM, Day 4 pre-resection: n=8, Days 6 and 13 post resection: n=5, Days 20 and 36: n=4, Day 50: n=3. **p<0.01, ***p<0.001).

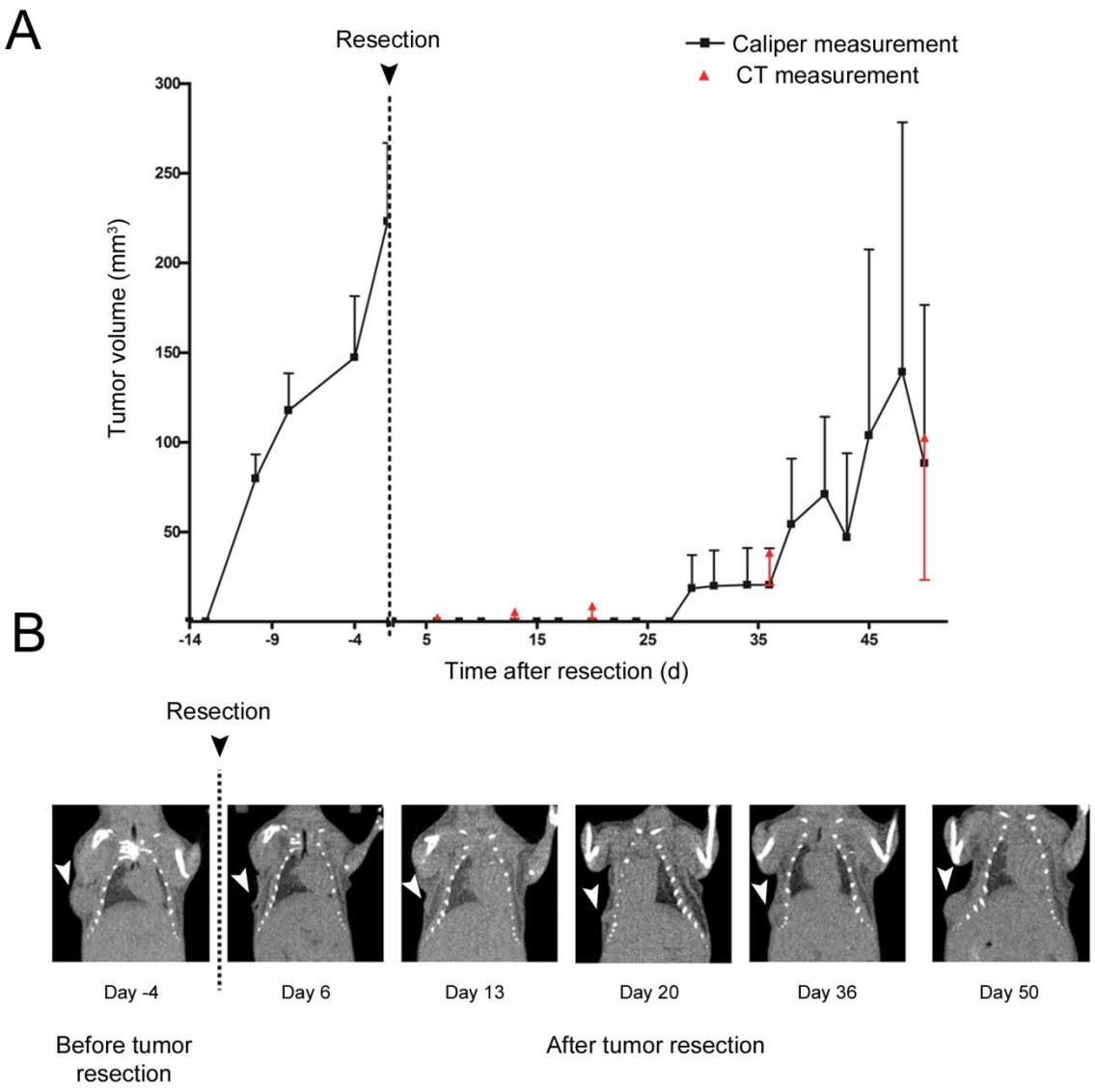

Figure 3. Detection of loco-regional tumor recurrence via CT and caliper measurements. (A) Growth curve of mean tumor volume obtained from caliper and CT measurements of the same group of animals, before and after primary tumor resection (mean±SEM, n=5 per study day, except days 20 and 36: n=4, day 50: n=3). **(B)** Coronal CT slices of a representative tumor-bearing mouse before and after resection show the presence (white arrow) and regrowth of the tumor after resection. Tumor growth was observed by CT from day 20 onwards.

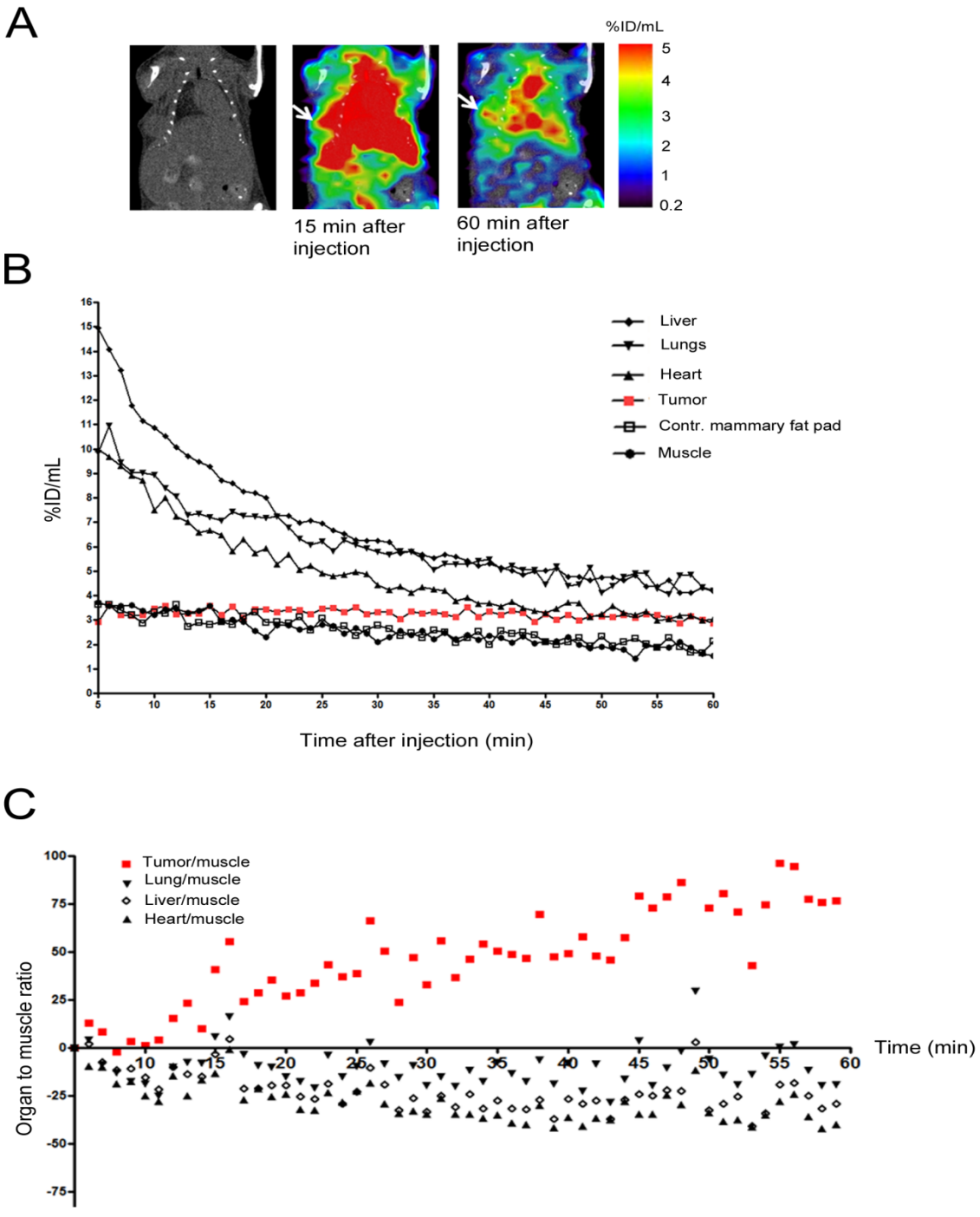

Figure 4. Biodistribution of [^{18}F]AH113804 in a recurrent HCC1954 tumor-bearing mouse. (A-left) Representative CT image of a HCC1954 xenograft mouse, acquired at Day 36 post resection. Recurrent tumor observed (White arrowhead). **(A- middle and right)** PET/CT at 15 min and 60 min p.i. of [^{18}F]AH113804, with retained radioactivity in the tumor visible by 60 min p.i.. **(B)** Dynamic ROI analysis of PET/CT shows a constant concentration at the tumor site but steady decline in all other organs (n=1). **(C)** Data of panel B normalized to the first time point show the relative change with a clear increase for tumor (n=1).

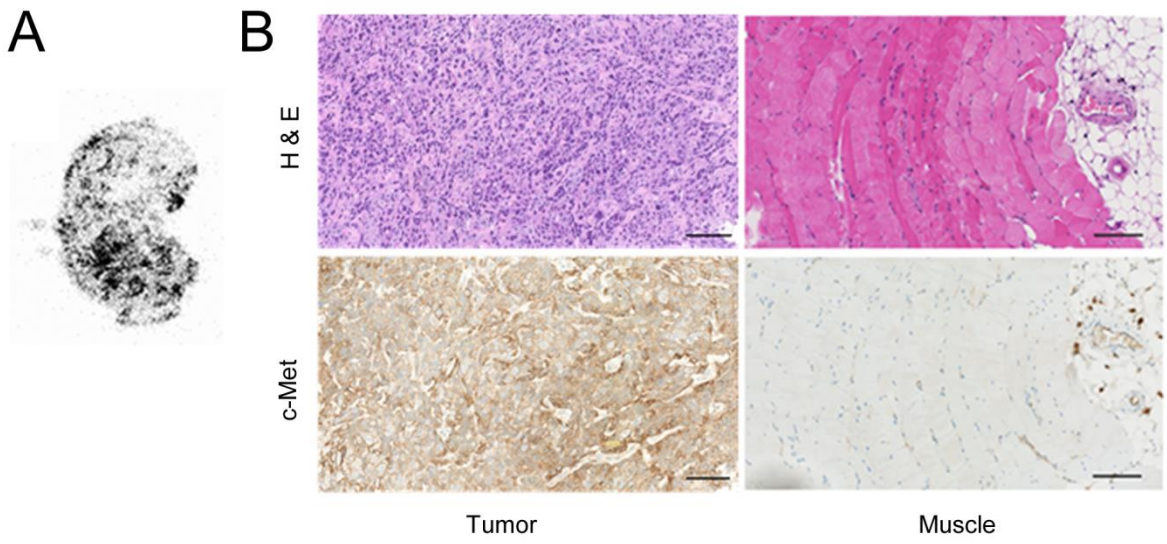

Figure 5. Autoradiography and immunohistochemistry demonstrate [^{18}F]AH113804 retention in c-Met positive HCC1954 tumor tissue.
(A) Autoradiography performed *ex vivo* on a resected tumor confirms retention of the [^{18}F]AH113804 radiotracer in tumor tissues. A heterogeneous distribution of tracer within the tumor section could be observed, not visible at the limited spatial resolution of PET imaging. **(B)** H&E staining (upper) and c-Met immunostaining (lower) of paraffin-embedded tumor and control skeletal muscle tissue (left and right columns respectively). H&E staining reveals the large, mitotic and disorganized phenotype characteristic of tumor cells, while immunohistochemistry reveals membranous c-Met staining in these cells. Scale bars=100 µm.

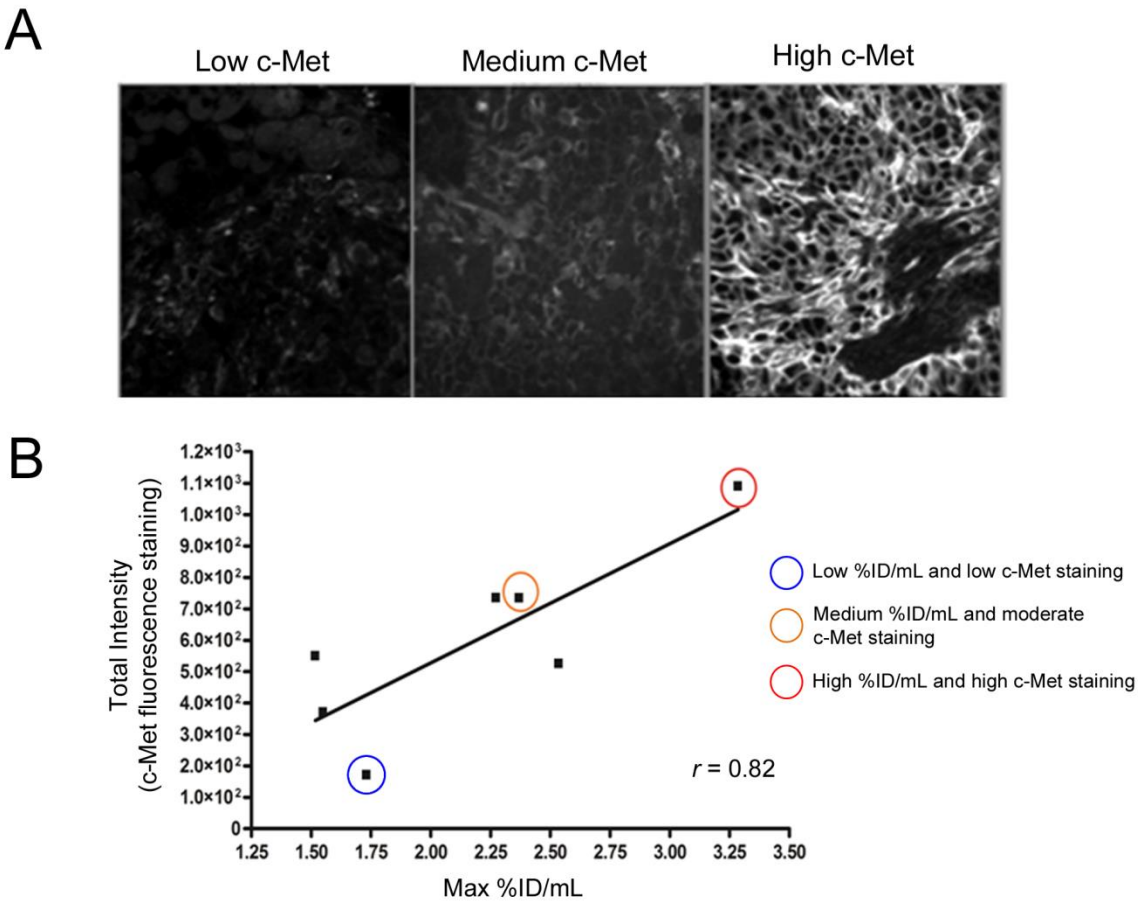

Figure 6. Uptake of [^{18}F]AH113804 correlate with the c-Met expression level in the corresponding resected tumor samples. (A) Immunofluorescent staining for c-Met in resected tumor samples (Day 14, n=7). Low, medium and high c-Met staining examples highlighted panel B. **(B)** A positive correlation is found between (a) the Max %ID/mL of tumor ROIs from *in vivo* PET images, and (b) the c-Met protein expression level from immunofluorescent staining in the same tumors after resection. Pearson's correlation coefficient=0.82 (P<0.05, n=7).

SUPPLEMENTARY MATERIAL

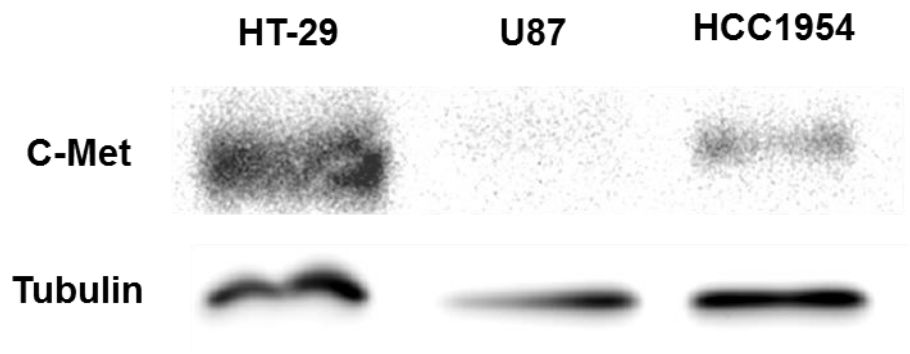

Suppl Fig 1. Western blot of c-Met expression. Highest expression level of c-Met is found in HT-29, less in HCC1954 and very little in U87 cell lysate. Tubulin was used as a loading control.

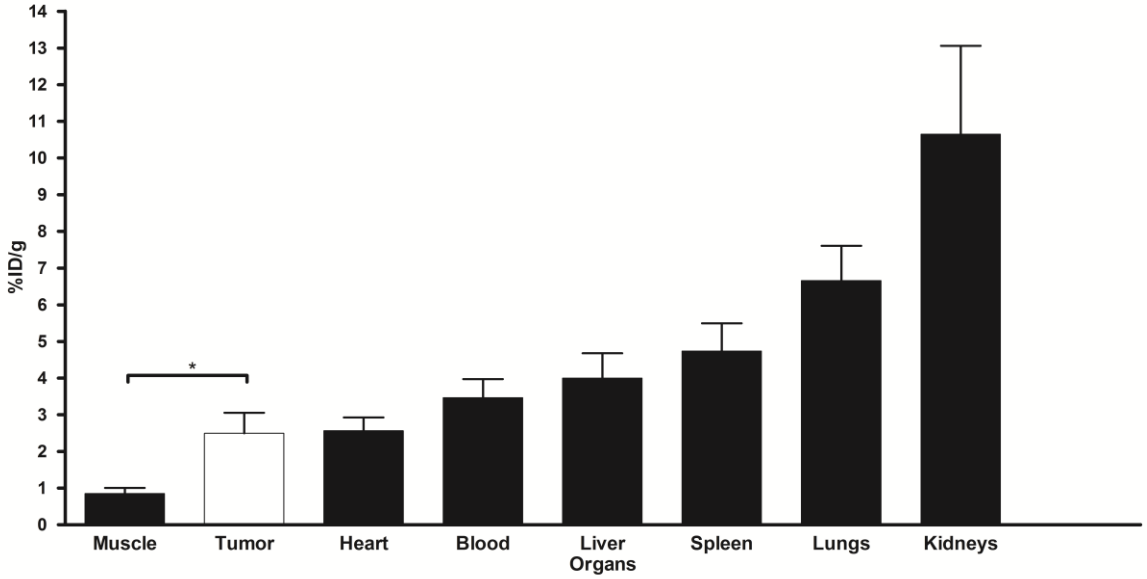

Suppl. Fig. 2 [^{18}F]AH113804 activity (% ID/g) from *ex vivo* assay of dissected organs and tissue samples from HCC1954 tumor bearing mice. Organs were excised at 70 min p.i. on Day 50 post tumor resection. A single *t*-test was performed to compare uptake of [^{18}F]AH113804 uptake in tumor and muscle. A statistically significant difference was observed ($p<0.05$, $n=3$). *P* value was calculated in R version 3.1.2.

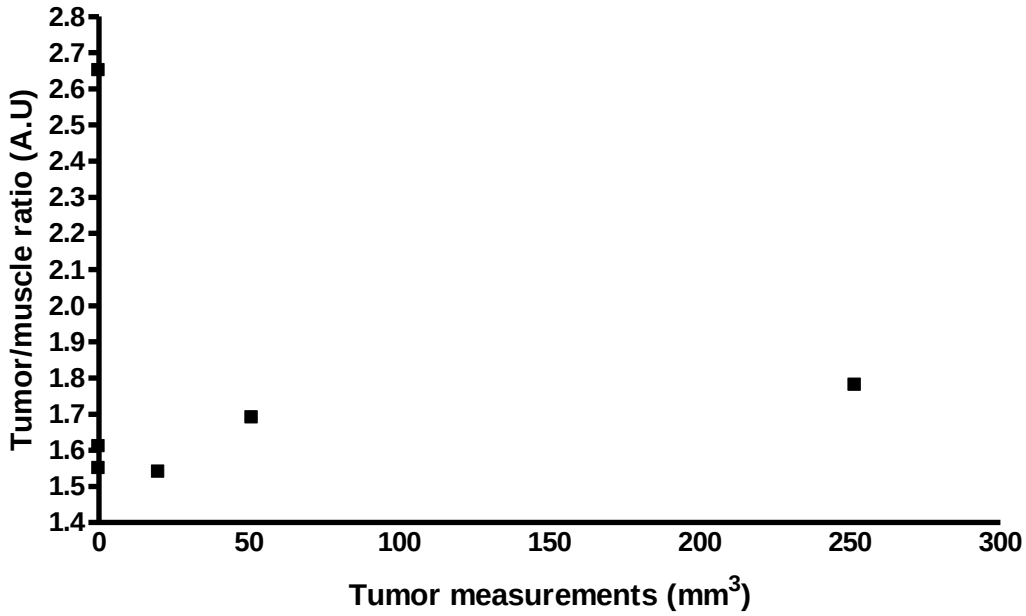

Suppl. Fig 3. No correlation observed between tumor size by caliper measurement and the uptake of the tracer at the tumor site. This graph shows the mean tumour measurement of all tumour-bearing mice at 6 timepoints, with its matching mean uptake of the tracer (measurement taken at day 4 pre tumor resection, day 0, day 6, day 13, day 20, day 36 and day 50 post tumor resection).

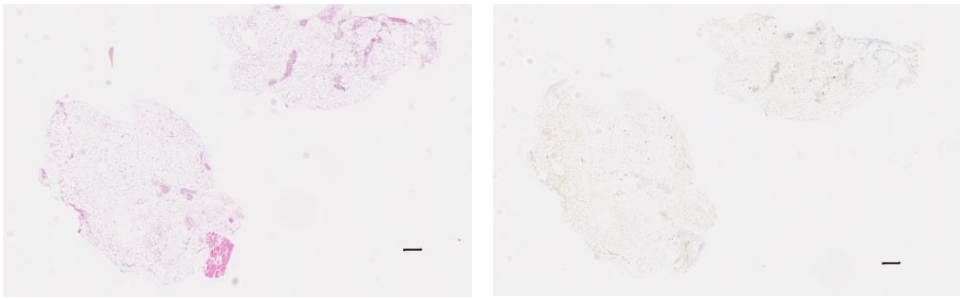

Suppl. Fig. 4. Immunohistochemical staining of mammary fat pad from a mouse that did not have a recurrent tumor after resection. The left panel represents the H&E staining of the sample that shows a clear presence of adipose tissue and ducts. No tumor cells were detected. The right panel shows staining for c-Met. No significant c-Met staining was observed. Scalebar represents 200 µm.

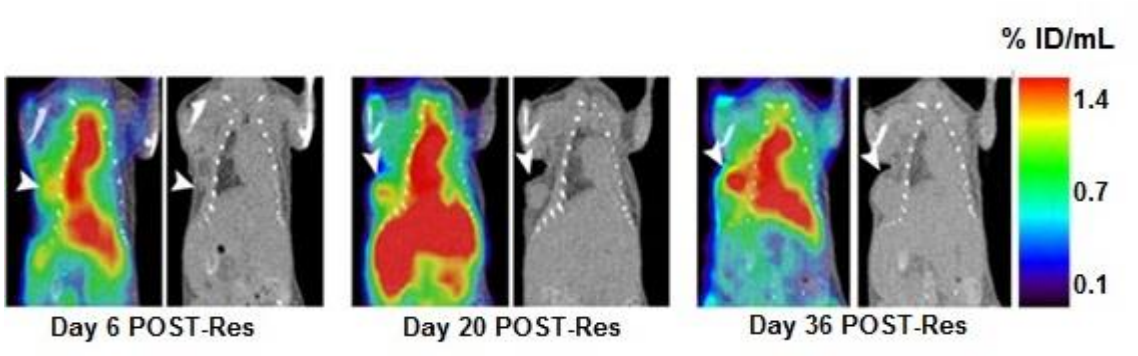

Suppl. Fig. 5. Progressive increase in uptake of [^{18}F]AH113804 at the tumor site post tumor resection. PET and CT image of a same tumor bearing mouse acquired on Day 6, Day 20 and Day 36 post resection showing uptake of [^{18}F]AH113804 at 60 min p.i. The recurrent tumour is clearly visible on the right flank of the animal (white arrowhead).

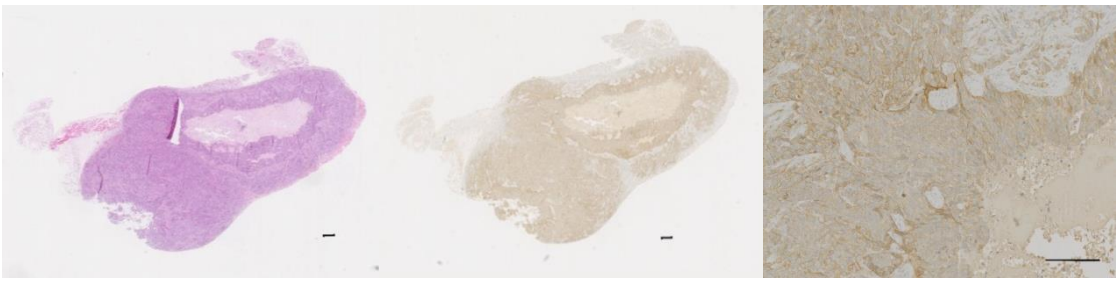

Suppl Fig 6: H&E staining E (left) and immunohistochemical staining for human c-Met (middle and right) on a representative tumour sample that was collected at day 14 post tumour inoculation. The tumour sample displays an area at its core devoid of cells. It also displays tumour cells at the periphery with fairly strong human c-Met staining. Presence of necrosis and membranous c-Met staining on tumor cells is visible on the right panel. Scalebars represent 200 µm.

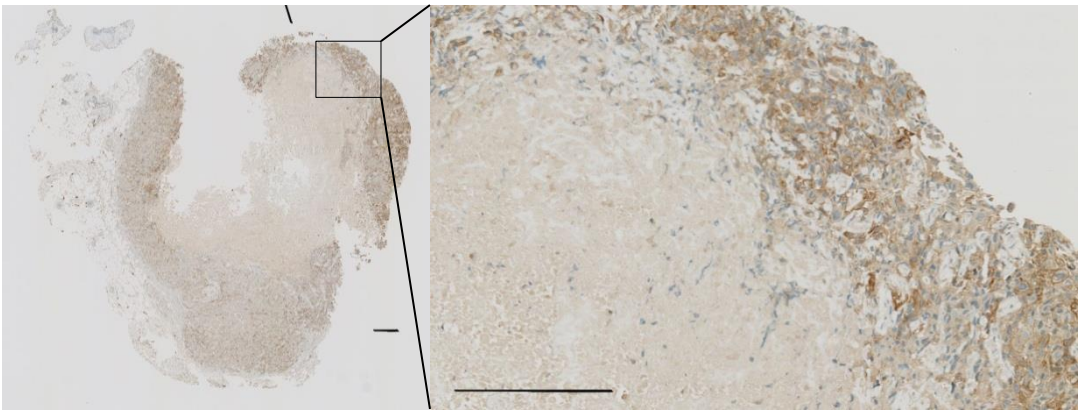

Suppl Fig 7. Immunohistochemical staining for c-Met on a representative recurrent tumor sample. Left panel shows the whole tumor sample while the right panel shows a magnified area of this tumor sample. The tumor sample displays a core of necrosis. The right panel shows membranous staining for c-Met around the tumor cells while the necrotic area shows no staining for c-Met. Scalebars represent 200 µm.

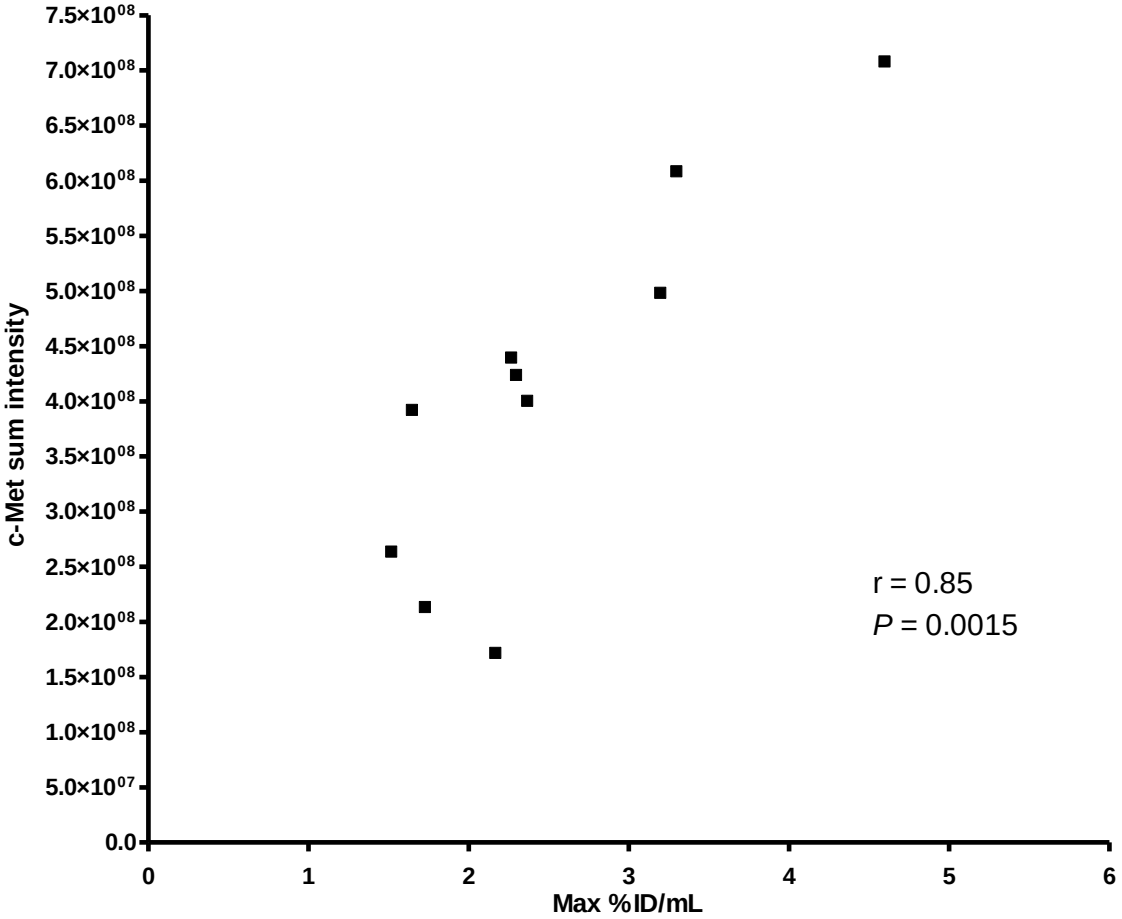

Supp Fig 8. Uptake of [^{18}F]AH113804 in tumors correlates with the c-Met expression level in samples of the same HCC1954 tumors. IHC detection of c-Met expression in FFPE preparation of tumor samples. Statistical analysis gave a Pearson's correlation coefficient of 0.85 (*P*= 0.0015, n = 10). Pearson *r* and *P* values were calculated in R version 3.1.2.

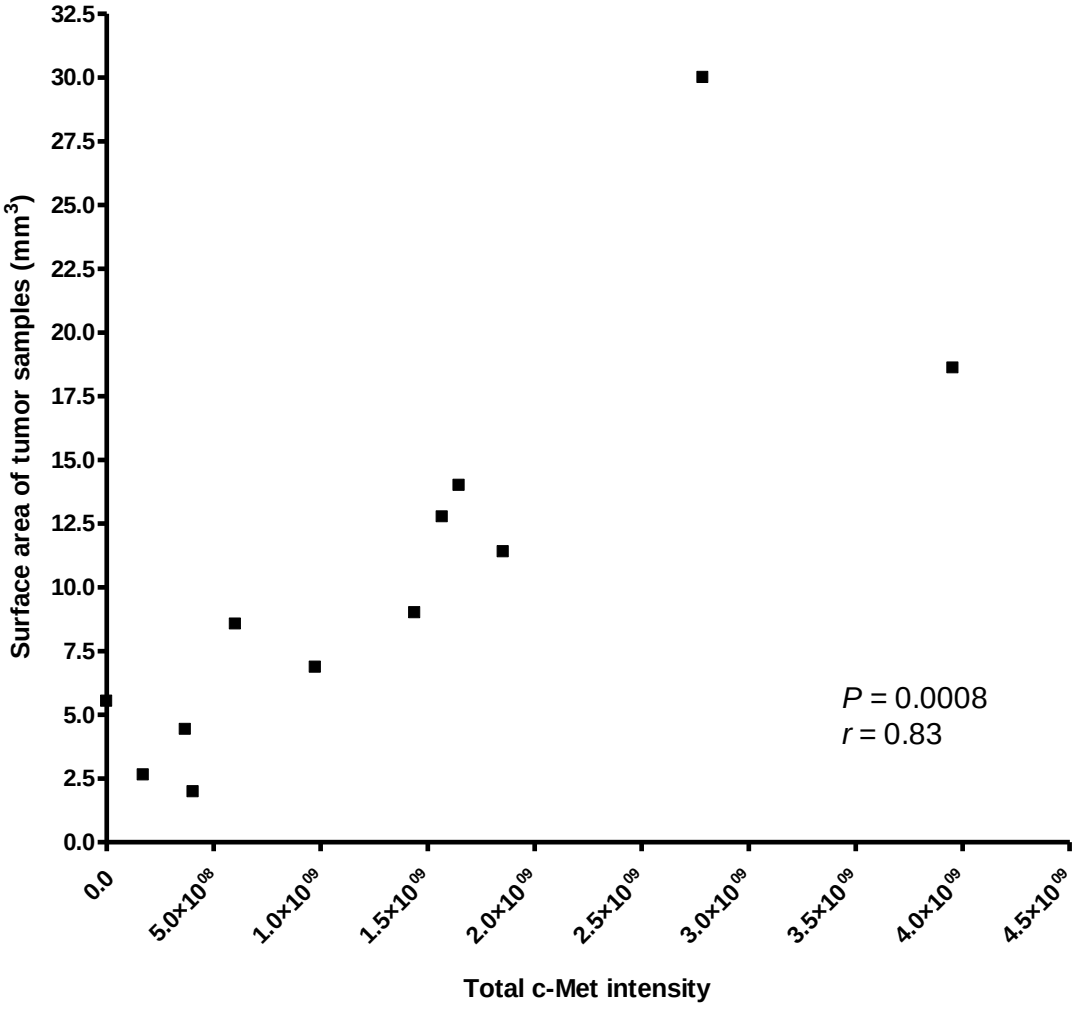

Suppl Fig 9 : Correlation between the surface area of viable tumour cells and the total c-Met intensity. The surface area measured includes areas with tumour cells only while excluding areas without cells, necrotic areas, and stroma. Statistical analysis gave a Pearson's correlation coefficient of 0.83 (*P* = 0.0008, n = 12). P and *r* values were calculated in R version 3.1.2.

A **B**

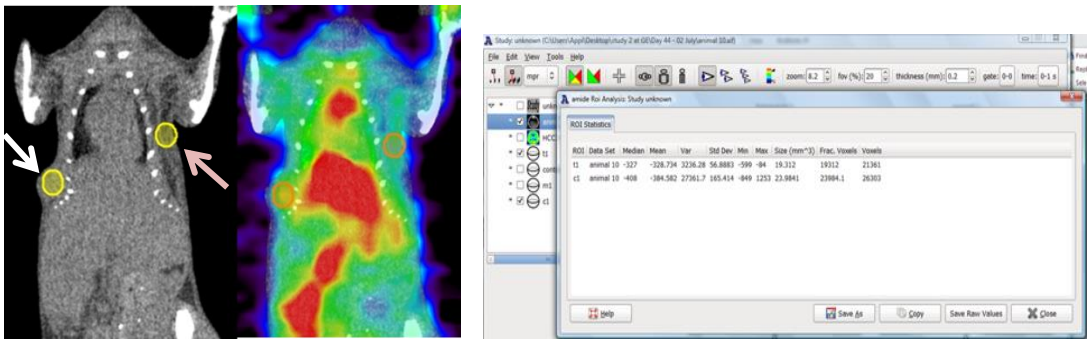

Suppl Fig 10: ROIs drawn in tumor and contralateral mammary fat pad. A. Representative CT (left) and CT/PET image (right) of HCC1954 tumour xenograft bearing mouse at day 36 post tumour resection. The ROI drawn at the tumour site (white arrow) was then replicated at the contralateral mammary fat pad (pink arrow) using the coronal and transverse section. **B.** ROI volumes for the tumour (t1) and the contralateral site (c1) are very similar. The ROI were drawn manually separately but attention was given to draw similar sized shape ROI for both sites and then checking that the volume of the respective ROI were very similar using the analysis section of the AMIDE software.

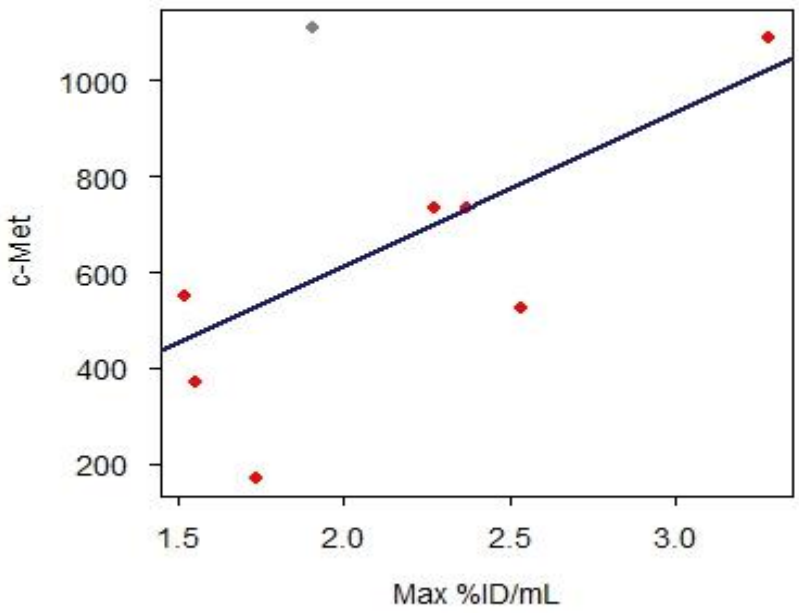

Suppl. Fig. 11. Identification of an outlier through the fitting of a regression line. Red dots fall between the upper and lower 1 percentile of all residuals while the grey dot is identified as an outlier. Statistical analysis performed in R version 3.1.2.

Day	MEAN (± SEM)	Lowest Individual Uptake Observed	Highest Individual Uptake Observed	n
-4	1.4 (0.2)	1.0	2.5	8
6	2.1 (0.1)	1.6	2.4	5
13	1.5 (0.2)	0.9	2.2	5
20	1.5 (0.3)	1.1	2.5	4
36	1.9 (0.7)	1.0	4.1	4
50	1.2 (0.3)	0.9	1.7	3

Supplementary Table 1. Uptake of radioactivity (%ID/mL) in HCC1954 tumors following [^{18}F]AH113804 administration, as determined by PET imaging.

PET Imaging timepoint	Number of mice imaged	Number of mice with recurrent tumors
10 days post implantation	8	N/A
6 days post resection	8	5
13 days post resection	8	5
20 days post resection	6	4
36 days post resection	6	4
50 days post resection	6	3

Supplementary Table 2. Number of mice used in this study and imaged at different PET imaging timepoints. Inclusion of the number of mice with visible recurrent tumors after tumor surgery.

Supplementary Methods:

Tumor xenograft model (continuation):

Initial PET scans with [^{18}F]AH113804 were acquired 10 days after tumor inoculation. Fourteen to sixteen days after tumor cell implantation, animals underwent surgery for tumor excision, and were subsequently allowed to recover under sufficient analgesia.

The animals were anaesthetized using 2.5% isofluorane in medical oxygen during the surgery. Area of the tumor site was cleaned using povidone-iodine. A 1 cm incision was then made around the tumor. A cotton swab was used to expose the tumor from the mammary fat pad. The tumor was then removed gently and completely from the mammary fat pad using scissors. In some cases, when the tumor was stuck to the skin, the skin was also removed to ensure that there would be no visible remnant of the tumor. Sham surgery was not performed on the contralateral mammary fat pad as the project license would not allow 2 surgeries to take place in one animal.

The animals were monitored for up to 50 days post tumor resection for local tumor recurrence, with PET imaging carried out on selected days post resection (Suppl. Table 2).

For autoradiography studies, female nude mice were inoculated with HC1954 cells in the second right mammary fat pad, according to the methods described above. Tumors were allowed to develop for 25 days before use.

Radiosynthesis of [^{18}F]AH113804 (continuation):

[^{18}F]AH113804 (chemical structure presented in Fig. 1A) was synthesized on a FASTlab automated synthesizer (GE Healthcare, Chalfont St Giles, UK) in a 2-step process. First, [^{18}F]fluorobenzaldehyde was synthesized from [^{18}F]fluoride and purified on a MCX+ (Mixed Cation Exchange, Waters) cartridge. Then, [^{18}F]fluorobenzaldehyde was conjugated to the peptide precursor and [^{18}F]AH113804 was purified and formulated.

[^{18}F]Fluoride was recovered from irradiated target water on a QMA cartridge (Waters) and then eluted using Kryptofix and $KHCO_3$ into a cyclic olefin copolymer reaction vessel and dried under a flow of nitrogen at 120 °C. Subsequent reaction with trimethylammonium benzaldehyde triflate in DMSO resulted in [^{18}F]fluorobenzaldehyde.

In the second step, the peptide precursor was dissolved in an aqueous solution of aniline hydrochloride and added to the purified [^{18}F]fluorobenzaldehyde to give crude [^{18}F]AH113804. Purification was done on a tC18 SPE (Solid Phase Extraction) cartridge with acetonitrile in PBS (21.4% v/v) followed by PBS to remove residual acetonitrile. [^{18}F]AH113804 was eluted into PBS (34 mL) from the tC18 cartridge with ethanol (2.4 mL) followed by PBS (2.6 mL) to give the formulated product (total volume 39 mL, ca. 6% EtOH).

CT and PET imaging:

Anesthesia (approximately 2% isoflurane in oxygen) was induced shortly before and maintained throughout imaging. PET imaging at 55-65 min post injection (pi) of [^{18}F]AH113804. A whole body CT scan followed (projection exposure time 400 ms, tube voltage 45 kVp). Animals were allowed to recover from anesthesia. Occasionally static PET imaging was replaced by a dynamic series at 5-65 min pi [^{18}F]AH113804.

PET data were attenuation and scatter corrected, then reconstructed by filtered back projection. Images were manually coregistered and analyzed by Regions of Interest (ROI) employing AMIDE (http://amide.sourceforge.net).

Imaging was performed at baseline (10 days post tumor inoculation, i.e. 4 days pre-resection) and on Days 6, 13, 20, 36 and 50 post tumor resection.

3D ellipsoid ROIs were placed on the tumor in CT images to estimate tumor volume (Suppl Fig 10). Additional ROIs were placed in skeletal muscle (left forelimb), liver, left and right kidney, and heart (blood pool). All ROI PET data were expressed as decay corrected radioactivity concentration normalized to the injected dose (% ID/mL).

Biodistribution of [^{18}F]AH113804 was obtained for the mice on the final imaging day (Day 50 post resection). Following PET/CT imaging, animals were sacrificed (approx. 70 min p.i.). Organs and tissues of interest were excised, weighed and radioactivity measured using a custom-built twin-crystal gamma counter. Ex vivo [^{18}F]AH113804 uptake is expressed as percentage radioactive dose per gram of tissue (% ID/g).

Autoradiography:

Autoradiography was performed on tumors harvested from nude mice 25 days after tumor inoculation. Mice were sacrificed 40 min after injection of approximately 7 MBq [^{18}F]AH113804 and corresponding PET imaging. Tumors were excised, snap frozen and cut into 8 µm thick sections. Sections were then imaged in a Micro Imager (Biospace Lab, Paris) which provides a spatial resolution of 25 µm for ^{18}F. Image acquisition duration was 90 min.

Histology:

Hematoxylin and eosin staining and c-Met immunohistochemistry were performed on consecutive 3µm thick tissue sections, employing the monoclonal rabbit antibody D1C1 (Ventana; diluted 1:30) against total c-Met. Antigen retrieval was employed (Standard Cell Conditioning 1/ Ventana). DAB (3,3'-diaminobenzidine) served as chromogen. Slides were processed with an automated system Ventana (BenchMark ULTRA, Roche, Switzerland), scanned with a Hamamatsu Nanozoomer 2.0 HT (Hamamatsu Photonics, Hamamatsu, Japan) and initially analyzed with Hamamatsu NDP.view2 viewing software. Quantitative analysis of the c-Met expression level was made using HistoQuest 4.2 (Tissugnostic, Vienna, Austria) software. IHC detection and quantification of c-Met expression in FFPE preparation of tumor samples are described in the section below.

Immunohistochemistry Data Analysis:

All the histological slides were digitalized at magnification x20 (0.46 µm/pixel) using Hamamatsu Nanozoomer 2.0 HT. Digital images in ndp format were submitted for quantitative image analysis using HistoQuest software. HistoQuest uses patented algorithms to detect the individual cells of interest and assesses intensity of antigens in the cell nucleus, membrane and cytoplasm. The program automatically detects tissue which is subjected to color separation module to differentiate between the blue and the brown shade. Nucleus detection algorithm on the hematoxylin shade was used to detect all cell nuclei and was defined as master channel. A ring mask around each nucleus was used to analyze the staining intensity of non-master chromogen (DAB) in given cellular location. The staining intensity is measured as mean intensity of all pixels of a cell and the range of values is from 0 to 255.

c-Met staining intensity was analyzed within 1.7 mm² regions of interest (ROI) that were visually identified over the tumor enriched region. Staining intensity was analyzed in ring masks

around each nucleus using an algorithm that identifies stained cytoplasmic and membranous areas. Raw data included minimum and maximum pixel value for every individual cell within the ROI. The average minimum and maximum pixel values were calculated for the whole region. The obtained data correlated with values acquired from PET scans.

Immunofluorescence:

Tissues were permeabilized and stained similar to the procedure outlined previously (*18*). A monoclonal rabbit c-Met antibody (1:100, D1C2, Cell signaling), followed by an incubation with a goat anti-rabbit Cy3 secondary antibody (1:500, Sigma), were used. Total fluorescence in each sample was measured and total c-Met-related intensity was corrected for differences between each animal using the same threshold. It was quantified using the software package TRI2 (Paul Barber, Oxford Institute for Radiation Oncology).

Statistical Analysis:

SEM was calculated to estimate the precision of the sample mean. Paired *t*-test of log-transformed TMRR was conducted to evaluate the difference between tumor and contralateral mammary fat pad uptake (Fig 2B). The correlation between total c-Met intensity from frozen tumor samples and the corresponding max %ID/mL for the uptake of [^{18}F]AH113804 at the tumor site (Fig 6B) is visualized with a scatter plot and Pearson correlation coefficients were calculated. The analysis was restricted to observations which fell between the upper and lower 5 percentile of all residuals, assigning any observation beyond this range as an outlier. This resulted in exclusion of one observation and the remaining seven observations were used in the final analysis (Suppl. Fig. 11). A two-sided P-value <0.05 was used to determine significance.